POLITECNICO DI TORINO
Repository ISTITUZIONALE

An Adaptive Backstepping Geometric Control for Spacecraft Attitude Dynamics with Unknown Inertia Parameters

Original
An Adaptive Backstepping Geometric Control for Spacecraft Attitude Dynamics with Unknown Inertia Parameters / Bertuccio, P., Sarvadon, J., Mancini, M., Capello, E.. - (2026), pp. 2409-2414. (American Control Conference 2026 New Orleans (USA) 26-29 May 2026).

Availability:
This version is available at: 11583/3014850 since: 2026-08-25T12:07:59Z

Publisher:
IEEE

Published
DOI:

Terms of use:

This article is made available under terms and conditions as specified in the corresponding bibliographic description in the repository

Publisher copyright
IEEE postprint/Author's Accepted Manuscript

©2026 IEEE. Personal use of this material is permitted. Permission from IEEE must be obtained for all other uses, in any current or future media, including reprinting/republishing this material for advertising or promotional purposes, creating new collecting works, for resale or lists, or reuse of any copyrighted component of this work in other works.

(Article begins on next page)

30 October 2026

An Adaptive Backstepping Geometric Control for Spacecraft Attitude Dynamics with Unknown Inertia Parameters

Pierantonio Bertuccio[1] and Jean-Luc Sarvadon[2] and Mauro Mancini[3] and Elisa Capello[4]

***Abstract*— This paper presents an adaptive backstepping controller formulated on the special orthogonal group SO(3), designed to address uncertainties in the spacecraft's inertia tensor without relying on gain scheduling. Taking advantage of the intrinsic Lie group-based attitude representation, the proposed controller provides adaptability to poorly modeled phenomena such as refueling, structural deployment, or damages. The effectiveness of the proposed controller is demonstrated both theoretically, through Lyapunov-based stability analysis, and numerically, via a simulation involving time-varying and unknown inertia, showing successful tracking of the desired reference attitude despite these difficulties. A comparison with a geometric PD tracking controller that includes feedforward and dynamic inversion demonstrates that the proposed adaptive approach is more accurate when the effort is comparable.**

I. INTRODUCTION

In recent years, the development of space manipulators capable of interacting with non-cooperative or unknown spacecraft have attracted growing interest from space agencies [1]. Indeed, space manipulators are the foundation for the realization of On-Orbit Servicing (OOS) missions, such as inspecting, capturing, refueling, and repairing satellites, assembling and maintaining large space infrastructure, and removing orbital debris [2]–[4]. All of these tasks create significant opportunities to improve cost efficiency and sustainability in the space economy. However, the field of OOS still faces considerable challenges that must be addressed, such as precise and safe manipulation of objects in harsh environments, uncertainties in object state estimation, motion planning, and feedback control. In particular, the attitude control systems of OOS manipulators must cope with external disturbances and significant time-varying uncertainties in the inertia tensor, due to interaction with non-cooperative targets and dynamic reconfiguration during manipulation activities. Attitude control of OOS robots is often addressed through robust control methodologies such as H_∞ [5] and Sliding Mode Control (SMC) [6]. Although robust control design guarantees stability and disturbance rejection under worst-case uncertainties and perturbations, this conservatism inevitably limits performance under milder operating conditions.

To overcome this drawback, adaptive control has emerged as a particularly promising strategy as it can effectively cope with large parametric uncertainties and time-varying dynamics. The interest in controllers capable of adapting to uncertainties in the inertia matrix is well documented in the literature. For instance, Panfeng Huang *et al.* [7] demonstrated the application of adaptive backstepping control for the capture of tethered, tumbling targets. Similarly, Wencheng Luo *et al.* [8] proposed inverse optimal adaptive control laws to address the attitude tracking problem of rigid spacecraft with uncertain inertia parameters. Ahmed et al. [9] designed a control law able to guarantee tracking of the attitude through a Lyapunov-based approach that doesn't require the knowledge of the inertia properties.

Most of the aforementioned adaptive control strategies rely on attitude representations based on quaternions or Euler angles. However, these parameterizations are inherently affected by well-known drawbacks: Euler angles suffer from singularities, while quaternions introduce a double coverage of the rotation group, which may lead to unwinding phenomena in control applications. In recent years, increasing attention has been devoted to geometric formulations that directly exploit the Lie group structure of rigid-body rotations. In particular, working on the special orthogonal group SO(3) provides a compact and non-redundant representation, free from singularities and ambiguities, and enables the design of control laws with stronger guarantees of global consistency and mathematical rigor.

Different authors investigated the advantages of an SO(3) representation, K. Zeyu *et al.* [10] proposed an adaptive attitude controller for a leader-folower formation on SO(3) to realize attitude consensus and attitude tracking through a sliding manifold. Furthermore, Yulin *et al.* [11] demonstrated a geometric backstepping control strategy for spacecraft attitude maneuvers based on a fixed-time fuzzy logic. Garanayak [12] validated a geometric adaptive SMC to effectively address disturbances and uncertainties in tracking the desired spacecraft attitude.

Motivated by these advances, this paper presents an adaptive backstepping controller for dynamical systems evolving on SO(3). The proposed controller enables precise attitude tracking without any prior knowledge of the inertia tensor, which is often imprecise, sensor-limited, or time-consuming to estimate [13]–[16]. Its adaptive nature ensures that the

*This publication is part of the project PNRR-NGEU which has received funding from the MUR – DM 630/2024

**This study was carried out within the SpaceItUp project funded by the Italian Space Agency,ASI,and the Ministry of University and Research,MUR,under contract n.2024-5-E.0-CUP n.I53D2400006000

[1]Pierantonio Bertuccio is with Department of Mechanical and Aerospace Engineering, Polytecnic of Turin, Turin, Italy (email:pierantonio.bertuccio@polito.it)

[2]Jean-Luc Sarvadon is with Department of Mechanical and Aerospace Engineering, Polytechnic of Turin, Turin, Italy in collaboration with Thales Alenia Space, Turin, Italy (e-mail: jeanluc.sarvadon@polito.it)

[3]Mauro Mancini is with Department of Mechanical and Aerospace Engineering, Polytecnic of Turin, Turin, Italy (e-mail: mauro.mancini@polito.it)

[4]Elisa Capello is with Department of Mechanical and Aerospace Engineering, Polytecnic of Turin, Turin, Italy (e-mail: elisa.capello@polito.it)

control law remains effective even when the inertia tensor varies due to events such as refueling, structural deployment, or damage, eliminating the need for explicit inertia estimation and enhancing operational flexibility.

For benchmarking purposes, the performance of the proposed controller is compared with a PD geometric tracking controller with feedforward dynamic inversion, without adaptation [17].

The remainder of the paper is organized as follows. Section II introduces the mathematical preliminaries and models used to simulate the attitude dynamics. Section III presents the proposed controller along with its stability proof, while Section IV reports the results of numerical simulations. Finally, concluding remarks and directions for future research are discussed in Section V.

II. Mathematical Preliminaries and Models

This section first gives the mathematical preliminaries on the Special Orthogonal Group SO(3). Then, the second part of the section presents the rotational kinematic and dynamic models of a rigid body evolving on SO(3).

A. Mathematical preliminaries

This subsection introduces the Special Orthogonal Group SO(3), which is used to parametrize the spacecraft attitude, and the associated Lie algebra. A brief overview of the relevant operators and maps is provided, while further details can be found in [REF].

The special orthogonal group $\mathrm{SO}(3)$ is the Lie group of rotation matrices in $\mathbb{R}^3$:

$$\mathrm{SO}(3) = \{R \in \mathbb{R}^{3\times 3} \mid R^\top R = I, \det(R) = 1\}.$$

Its Lie algebra $\mathfrak{so}(3)$ consists of skew-symmetric matrices as follows:

$$\mathfrak{so}(3) = \{\widehat{\Omega} \in \mathbb{R}^{3\times 3} \mid \widehat{\Omega}^\top = -\widehat{\Omega}\},$$

where $\widehat{\cdot}: \mathbb{R}^3 \to \mathfrak{so}(3)$ maps a vector $\Omega = [\Omega_1, \Omega_2, \Omega_3]^\top$ to a skew-symmetric matrix $\hat{\Omega}$:

$$\widehat{\Omega} = \begin{bmatrix} 0 & -\Omega_3 & \Omega_2 \\ \Omega_3 & 0 & -\Omega_1 \\ -\Omega_2 & \Omega_1 & 0 \end{bmatrix}.$$

Then, the vee map $(\cdot)^\vee$ provides the inverse, making the Lie algebra $\mathfrak{so}(3)$ isomorphic to $\mathbb{R}^3$ via the hat $\widehat{(\cdot)}$ and vee $(\cdot^\vee)$ maps.

The exponential map $\exp : \mathfrak{so}(3) \to \mathrm{SO}(3)$ reconstructs a rotation matrix from a skew-symmetric matrix:

$$\exp(\widehat{\Omega}) = I + \frac{\sin\|\Omega\|}{\|\Omega\|}\widehat{\Omega} + \frac{1-\cos\|\Omega\|}{\|\Omega\|^2}\widehat{\Omega}^2,$$

where $\|\Omega\| = \sqrt{\Omega_1^2 + \Omega_2^2 + \Omega_3^2}$. This map is surjective and locally bijective for $\|\Omega\| < \pi$. Its inverse, the logarithmic map, is:

$$\log(R) = \frac{\theta}{2\sin\theta}(R - R^\top), \quad \theta = \cos^{-1}\left(\frac{\mathrm{tr}(R)-1}{2}\right),$$

which is valid for all the elements of the subset:

$$\{R \in SO(3) \mid \mathrm{tr}(R) = -1\}.$$

For a one-parameter subgroup $R(t) = \exp(t\widehat{\Omega})$, the derivative of the logarithmic map gives the angular velocity in skew-symmetric matrix representation [18]:

$$\frac{d}{dt}\log(R(t)) = \widehat{\Omega}.$$

Finally, the trace operator $\mathrm{tr}(\cdot)$ induces the Frobenius inner product $\langle A, B\rangle_{tr} := \langle A, B\rangle_F = \mathrm{tr}(A^\top B) = \mathrm{tr}(BA^\top)$ and the Frobenius norm $\|A\|_F = \sqrt{\langle A, A\rangle_F}$, with $\mathrm{tr}(\boldsymbol{a}\boldsymbol{b}^\top) = \boldsymbol{a}^\top\boldsymbol{b}$. for real column vectors. In the following paper, the explicit time dependence of variables (e.g., $x(t)$) will be omitted when clear from context.

B. Mathematical models

This subsection presents the rigid-body attitude kinematics and dynamics on SO(3). Subsequently, the attitude error dynamics are derived, and the control objective is stated.

Consider the non-linear dynamical system:

$$\dot{R} = R\widehat{\Omega}, \tag{1a}$$

$$J\dot{\Omega} = -\Omega^\wedge J\Omega + \boldsymbol{\tau}, \tag{1b}$$

where $R \in \mathrm{SO}(3)$ is the rotation matrix representing the orientation of the body-fixed frame attached to the spacecraft with respect to an inertial frame in $\mathbb{R}^3$. Then, $\Omega \in \mathbb{R}^3$ is the angular velocity vector expressed in the body-fixed frame, while $J \in \mathbb{R}^{3\times 3}$ is the inertia tensor of the rigid body, symmetric and positive-definite, and here assumed completely unknown. Also, $\boldsymbol{\tau} \in \mathbb{R}^3$ is the external torque vector applied to the body, expressed in the body-fixed frame. Let R_d and Ω_d denote the evolution of the desired attitude over time. Then, the attitude error R_e and angular velocity error Ω_e are defined as:

$$R_e = R_d^\top R, \tag{2a}$$

$$\Omega_e = \Omega - R^\top R_d \Omega_d. \tag{2b}$$

Remark 1: The Special Orthogonal group $\mathrm{SO}(3)$ is a compact, non-contractible manifold, which carries a topological obstruction preventing the existence of a smooth, continuous feedback law that renders a single equilibrium globally asymptotically stable [22]. However, since the pointing task can always be formulated in terms of the orientation error $R_e = R_d^\top R$, the control objective reduces to stabilizing R_e to the identity I. This formulation allows for almost-global convergence, i.e., convergence for all

$$R_e \in SO(3)/\mathcal{O}, \qquad \mathcal{O} = \{R_e \in SO(3) \mid \mathrm{tr}(R_e) = -1\},$$

which corresponds to the set of 180-degree rotations where the matrix logarithm is not uniquely defined. Therefore, the subsequent control design and stability results are consistent with this fundamental topological limitation.

The error kinematics and dynamics are derived from the system (1a)–(1b) as:

$$\dot{R}_e = R_e\widehat{\Omega_e}, \tag{3a}$$

$$\tilde{J}\dot{\Omega}_e = -\Omega^\wedge \tilde{J}\Omega + \boldsymbol{\tau} + \tilde{J}\left(\widehat{\Omega}R^\top R_d\Omega_d - R^\top R_d\dot{\Omega}_d\right). \tag{3b}$$

It is possible to rewrite (3b) in a form inspired by plants controllable by nonparametric Model Reference Adaptive Control (MRAC) systems:

$$\dot{\Omega}_e = \Lambda[\boldsymbol{\tau} + \Theta^\top \Phi], \tag{4}$$

$$\Phi = \begin{bmatrix} -\Omega_y\Omega_z; -\Omega_z\Omega_x; -\Omega_x\Omega_y; -\Omega_x^2; -\Omega_y^2; -\Omega_z^2; \\ \hat{\Omega}R^\top R_d\Omega_d - R^\top R_d\dot{\Omega}_d + k_r e_\omega \end{bmatrix} \tag{5}$$

such that the matched uncertainties in the model are collected inside a term $\Theta^T\Phi$, where $\Theta \in \mathbb{R}^{9\times 3}$ is a coefficient matrix and $\Phi \in \mathbb{R}^{9\times 1}$ is the regressor vector representing the functional form of the matched uncertainties. $\Lambda \in \mathbb{R}^{3\times 3}$ denotes the matrix capturing the uncertainty on the control channel (in this case related to the inertial properties multiplying the control torque). Λ is assumed symmetric, positive definite, and invertible, but completely unknown. However, Λ is supposed to be uniformly bounded, so that $\lambda_{\min} I \leq \Lambda \leq \lambda_{\max} I$ is satisfied for with $0 < \lambda_{\min} \leq \lambda_{\max} < \infty$. The control objective is to guarantee that the attitude of the spacecraft asymptotically converges to the desired one, namely $R_e \to I$ and $\Omega_e \to 0$ as $t \to \infty$, while achieving this goal without any prior knowledge of the inertia matrix, which is assumed completely unknown.

III. Adaptive Backstepping Controller on SO(3)

This section details the control strategy employed to track the reference attitude. The design follows the classical backstepping approach, and the stability of the closed-loop system is validated through rigorous Lyapunov analysis.

First, the control torque is computed by the following equation:

$$\tau = -K_r \log(Re)^\vee - K_w z + \hat{\Theta}^\top \Phi, \tag{6}$$

where K_r and K_w are two arbitrary positive gains and Φ is the regressor vector. Then, the parametric adaptive gain matrix $\hat{\Theta}$ is updated in real-time according to the following law:

$$\dot{\hat{\Theta}} = \Gamma_\Theta \Phi z^\top, \tag{7}$$

where Γ_Θ denotes arbitrary, symmetric, and positive definite adaptive rate matrices. Finally, z is defined as:

$$z = \Omega - \beta, \tag{8}$$

where $\beta : SO(3) \to \mathfrak{so}(3)$ is a smooth virtual control input as follows:

$$\begin{aligned} \beta &= -K_r log(R_e) + (R^T R_d \Omega_d)^\wedge \\ &= -K_r log(R_e)^\vee + R^T R_d \Omega_d \end{aligned} \tag{9}$$

The proposition below characterizes the stabilizing role of the virtual control input β.

Proposition 1: Let $R_e \in SO(3)$ denote the orientation error as in Eq. (2a), with dynamics given by Eq. (3a). For all

$$R_e \in SO(3)/\mathcal{O}, \quad \mathcal{O} = \{R_e \in SO(3) \mid \mathrm{tr}(R_e) = -1\},$$

the trajectories of (3a), under the virtual control input β in Eq. (9), asymptotically converge to $R_e = I$.

Proof: Consider the Lyapunov candidate

$$V_1(R_e) = \tfrac{1}{2} K_r \langle \log(R_e), \log(R_e) \rangle_{tr}, \quad K_r > 0,$$

which is positive definite with respect to $R_e = I$. Differentiating along the trajectories of (3a) yields

$$\begin{aligned} \dot{V}_1(R_e) &= K_r \langle \log(R_e), \widehat{\Omega}_e \rangle_{tr} \\ &= K_r \langle \log(R_e), \widehat{\Omega} - (R^T R_d \Omega_d)^\wedge \rangle_{tr} \end{aligned} \tag{10}$$

where (2b) is used. Substituting (9) into (10) yields

$$\dot{V}_1(R_e) = K_r \langle log(R_e), -K_r log(R_e) \rangle_{tr}, \tag{11}$$

which can be rewritten as

$$\dot{V}_1(R_e) = -K_r^2 \langle log(R_e), log(R_e) \rangle_{tr} \tag{12a}$$

$$\dot{V}_1(R_e) = -K_r V_1. \tag{12b}$$

which is negative definite for all $R_e \neq I$. Since $V_1 > 0$ and $\dot{V}_1 < 0$ are satisfied everywhere except at the equilibrium $R_e = I$, the proof is complete. ∎

Now, the convergence properties of the closed-loop system (3), (6)-(9) are stated in the following theorem.

Theorem 1: Consider the orientation errors defined in (2), whose evolution is given by the error system (3). Assume that the control law (6) with the kinematic virtual input (9) and the adaptive law (7) are applied. Then, for all

$$R_e \in SO(3)/\mathcal{O}, \qquad \mathcal{O} = \{R_e \in SO(3) \mid \mathrm{tr}(R_e) = -1\},$$

the closed-loop trajectories satisfy

$$R_e(t) \to I, \qquad z(t) \to 0, \qquad \Delta\Theta(t) \text{ is bounded},$$

as $t \to \infty$, where $z = \Omega - \beta$ and $\Delta\Theta = \hat{\Theta} - \Theta$.

Proof: Define the composite Lyapunov candidate

$$V_c(R_e, z, \Delta\Theta) = V_1(R_e) + \tfrac{1}{2} z^\top \Lambda^{-1} z + \mathrm{tr}\big(\Delta\Theta^\top \Gamma_\Theta^{-1} \Delta\Theta\big),$$

where $V_1(R_e) = \frac{1}{2} K_r \langle \log(R_e), \log(R_e) \rangle_{\mathrm{tr}}$ is the candidate used in Proposition 1, $K_r > 0$, $K_w > 0$, and Λ is positive definite. Differentiating V_c along the closed-loop dynamics yields:

$$\begin{aligned} \dot{V}_c(R_e, z, \Delta\Theta) = K_r \langle log(R_e), (\Omega - R^\top R_d \Omega_d)^\wedge \rangle_{tr} + \\ + z^\top(\boldsymbol{\tau} + \Theta^\top \Phi) + tr(\Delta\Theta^\top \Phi z^\top). \end{aligned} \tag{13}$$

Then, substituting (6) and (7) and using (8) the following results are obtained:

$$\begin{aligned} \dot{V}_c(R_e, z, \Delta\Theta) &= -K_r V_1 + K_r \langle log(R_e), \widehat{z} \rangle_{tr} + \\ &\quad z^\top(-K_r log(Re)^\vee - K_w z + \Delta\Theta^\top \Phi) + \\ &\quad - tr(\Delta\Theta^\top \Phi z^\top). \\ &= -K_r V_1 + z^\top(K_r log(Re)^\vee) \\ &\quad + z^\top(-K_r log(Re)^\vee - K_w z + \Delta\Theta^\top \Phi) + \\ &\quad - tr(\Delta\Theta^\top \Phi z^\top) \\ &= -K_r V_1 - K_w z^\top z + z^\top(\Delta\Theta^\top \Phi) + \\ &\quad - tr(\Delta\Theta^\top \Phi z^\top). \end{aligned} \tag{14}$$

Finally, using the properties of the trace operator

$$\dot{V}_c(R_e, z, \Delta\Theta) = -K_r V_1(R_e) - K_w z^\top z \leq 0. \tag{15}$$

Hence $V_c(t) \leq V_c(0)$ for all $t \geq 0$, which implies that $V_1(R_e(t))$, $z(t)$ and $\Delta\Theta(t)$ remain bounded for all $t \geq 0$. The map $\dot{V}(R_e, z, \Delta\Theta)$ is continuously differentiable, and the time derivatives are as follows:

$$\begin{aligned}\ddot{V}_c(R_e, z, \Delta\Theta) = K_r \left\langle \log R_e,\, z - K_r \log R_e \right\rangle_{\mathrm{tr}} + \\ + z^\top \left(-K_r \log R_e - K_w z + \Delta\Theta^\top \Phi\right).\end{aligned} \tag{16}$$

Since $\log R_e(t)$, $z(t)$, and $\Delta\Theta(t)$ are bounded, $\ddot{V}$ is also bounded. Invoking Barbalat's lemma [20], we get

$$\lim_{t\to\infty} \dot{V}(R_e, z, \Delta\Theta) = 0. \tag{17}$$

By Proposition 1, it follows that $V_1(R_e(t)) \to 0$, i.e., $R_e(t) \to I$. Substituting this into (15) yields $\dot{V}_c = -K_w z^\top z$, and this guarantees that $z(t) \to 0$ as $t \to \infty$. Finally, boundedness of $\Delta\Theta(t)$ follows from the boundedness of V_c. ■

IV. Numerical Simulations

This section describes the case study and provides the results of the numerical simulations. Here, the controller described in the previous section is put into comparison with the constant-gain PD geometric controller from [17].

A. Case study

The case study selected to test the proposed control strategy is the capture of a tumbling orbital debris with unknown inertia parameters. The capture strategy is structured in the following phases: 1) *Initial alignment:* the spacecraft manipulator is assumed to be in the proximity of the debris, aligned with its angular momentum direction. 2) *Relative angular motion reduction:* the space robot acquires an angular velocity to reduce the relative angular motion with respect to the tumbling debris. 3) *Robotic manipulator deployment:* the robotic arms are deployed from their initial retracted configuration to a planned capture position. 4) *Contact point approach:* once the relative motion and attitude are reduced below a designated threshold, the robot manipulators move the end-effectors toward the target contact points to complete the capture. 5) *Post-capture detumbling:* after contact, the coupled system (space manipulator + debris) undergoes detumbling.

This sequence of operations naturally involves large variations in the system inertia parameters and in the angular velocities to be tracked. To highlight these effects, the capture phases are implemented in MATLAB/Simulink as follows:

- $t \in [0, 500]$: The spacecraft starts from zero angular velocity, while the desired angular rate is set to $[n, -10n, 2n]^\top$ [rad/s] to perform the capture maneuver, with n denoting the orbital angular velocity. In this phase, the inertia is constant and equal to J_0 as defined in Eq. (19).
- $t \in [500, 2600]$: The inertia properties vary according to the law in Eq. (18), simulating the deployment of a robotic appendage or capture equipment. Specifically, the inertia is J_0 at $t = 500$ and converges exponentially to J_1 in Eq. (19).
- $t \in [2600, \text{end}]$: An instantaneous docking occurs with the target, resulting in an abrupt change in the inertia matrix from J_1 to J_2 in Eq. (19). After docking, the control objective is to drive the angular velocity of the combined body to zero, effectively simulating the detumbling of the captured debris. The time evolution of the inertia values are further shown in Figure 1, with the different mission phases highlighted.

$$J = J_0 * (1 - 0.5 * e^{(t-t_0)}), \quad t_0 = 500 \tag{18}$$

$$J_0 = \underbrace{\begin{bmatrix} 625 & 5.5 & 3 \\ 5.5 & 350 & 4 \\ 3 & 4 & 1000 \end{bmatrix}}_{\text{Initial inertia matrix}}$$

$$J_1 = \underbrace{\begin{bmatrix} 1250 & 11 & 6 \\ 11 & 700 & 8 \\ 6 & 8 & 2000 \end{bmatrix}}_{\text{Final inertia matrix before capture}} \tag{19}$$

$$J_2 = \underbrace{\begin{bmatrix} 3945.4 & 66.7 & 12.8 \\ 66.7 & 3663.5 & 160 \\ 12.8 & 160 & 2011.8 \end{bmatrix}}_{\text{Total inertia matrix after capture}}$$

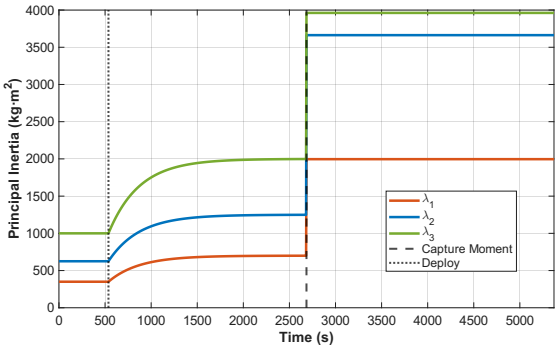


Fig. 1. Inertia variation

By considering these diverse scenarios within a single simulation framework, it becomes possible to evaluate how the proposed adaptive controller responds to inertia variations under fast rotational dynamics imposed by the capture maneuver. This condition emphasizes the uncertain and time-varying nature of the inertia parameters, making the case study a meaningful benchmark against the constant-gain PD geometric controller from [17], which does not account for such variations.

Furthermore, the simulations are carried out under the assumption that both controllers have no knowledge of the inertia matrix, which is replaced by the identity matrix in the control law implementation. The integration step is set to 0.01 seconds, with a fourth-order Runge–Kutta scheme used for numerical integration. The controller parameters employed in the simulations are shown in Table I.

TABLE I

CONTROLLER PARAMETERS

Parameter	Symbol
PD Controller	
K_r	0.5714
K_w	25
Adaptive Controller	
K_r	0.005
K_w	75
Γ_Θ	$\mathbf{I}_{9\times 9} \times 1e8$

B. Numerical Results

This section presents the numerical results obtained by simulating the capture scenario described in Section IV-A. The results are reported in graphical form, showing the evolution of angular velocities, tracking errors, and control inputs across the different capture phases. Particular emphasis is placed on evaluating how each controller manages the abrupt and gradual inertia variations induced by manipulator deployment and post-docking dynamics. The scenario is subject to generic disturbances modeled as white noise plus a low frequency sinusoid acting equally on all axis:

$$d(k) = 0.1\sin(0.001\,k\,dt) + 0.025\,\eta, \quad \eta \sim \mathcal{N}(0,1) \quad (20)$$

Figures 2 and 3 show the results of the numerical simulations in terms of angular velocity tracking performance. In Fig. 2, the desired angular velocities (dotted line) are compared with the trajectories obtained using the proposed adaptive controller (solid line) and the constant-gain PD geometric controller from [17] (dashed line). Figure 3 shows the corresponding tracking errors for the three components.

The results clearly demonstrate that the PD controller fails to track the desired angular velocities during Phases 1 and 2, when the objective is to follow the fast rotational dynamics of the target. In these intervals, significant tracking errors appear in all components, with the most pronounced mismatch occurring along the z-axis, where the inertia assumes its largest value. In this direction, the angular velocity achieved under PD control approximately doubles the reference value. This discrepancy arises because the nominal controller cannot compensate for uncertain and time-varying inertia: the lack of precise inertia knowledge prevents accurate dynamic inversion, leading to systematic tracking errors.

In contrast, the adaptive controller achieves accurate tracking across all axes, maintaining performance despite parametric uncertainty and rapid variations in the inertia tensor. From a practical standpoint, the poor tracking of the PD controller in Phases 1 and 2 would result in an incomplete reduction of the relative motion between the chaser and the target, potentially compromising the capture maneuver. Moreover, these results highlight how unknown and time-varying inertia properties become particularly critical in fast rotational regimes, where the proposed adaptive controller proves effective by maintaining performance without requiring explicit inertia estimation.

In Phase 3, corresponding to the post-docking detumbling task, both controllers succeed in driving the angular velocity to zero. This outcome confirms that the main advantage of the adaptive strategy emerges in the presence of rapid, inertia-dependent dynamics, while in quasi-static conditions the difference with the PD controller becomes less pronounced. Next, the control torques required by each controller are analyzed to complement the previous discussion on angular velocity tracking. It is worth noting that both controllers were tuned so that the integrated squared norm of the applied torque remains more or less comparable, providing a fair basis for comparison.

TABLE II

RMSE COMPARISON

	PD Controller	Adaptive Controller
RMSE $[rad/s]$	4.024e-3	2.776e-3
Effort $[N^2m^2/s]$	155.61	143.10
RMSE comparison (%)	–	-55.55
Effort comparison (%)	–	-7.96

Fig. 4 depicts the control torque profiles along the three axes throughout the entire mission, while Fig. 5 reports the corresponding torque norms. It can be observed that the adaptive controller exhibits slightly more aggressive behavior at the onset of each maneuver, particularly during rapid transients. The nominal PD controller, on the other hand, generates less responsive torque profiles, which explains its poor tracking performance in Phases 1 and 2. Increasing the proportional gain would partially mitigate this issue, as it would improve convergence to the desired angular velocity, but at the expense of substantially higher torque effort throughout the entire control process.

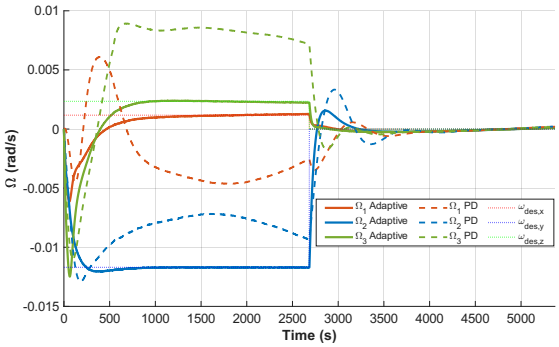


Fig. 2. Angular velocity comparison

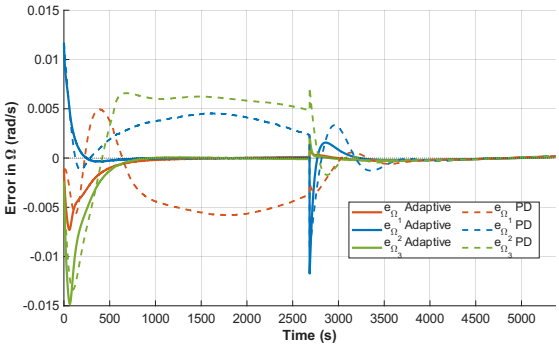


Fig. 3. Angular velocity tracking error before capture

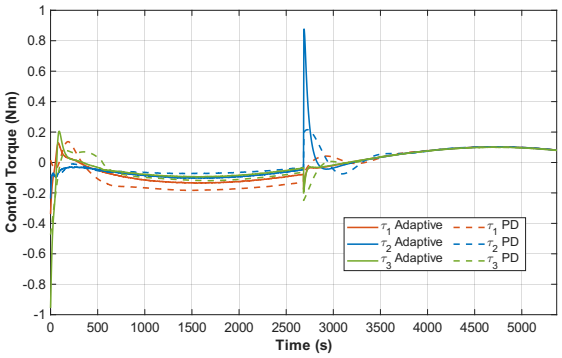


Fig. 4. Torque comparison

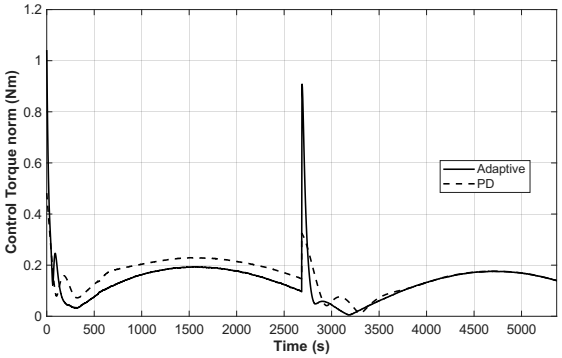


Fig. 5. Torque norm comparison

V. CONCLUSIONS

This paper has presented a novel adaptive back-stepping controller formulated directly on the SO(3) manifold for spacecraft attitude tracking under significant inertia uncertainties. The proposed control law eliminates the need for gain scheduling by continuously adapting to parametric uncertainties, demonstrating robustness against poorly modeled dynamics arising from events such as robotic arm deployment, refueling, or instantaneous docking. Theoretical analysis establishes the asymptotic stability of the closed-loop system, while numerical simulations confirm the controller's effectiveness and demonstrate its advantages over a non-adaptive geometric PD scheme. In particular, the adaptive controller improves tracking accuracy under uncertain and time-varying inertia, while maintaining moderate control effort, thereby enhancing overall control efficacy. This work serves as a preliminary study on the applicability of the proposed control approach for complex missions characterized by difficult-to-model or unknown inertial properties. Future extensions are already planned, including numerical testing in a higher-fidelity simulation environment that incorporates actuator and sensor models, comparison with different control algorithms and also robustness analysis based on Monte Carlo simulations.

Finanziato dall'Unione europea NextGenerationEU | Ministero dell'Università e della Ricerca | Italiadomani

REFERENCES

[1] D. Fourie, B.E. Tweddle, S. Ulrich and A. Saenz-Otero, "Flight Results of Vision-Based Navigation for Autonomous Spacecraft Inspection of Unknown Objects", *Journal of Spacecraft and Rockets*, vol. 51, no. 6, pp 2016-2016, 2014, doi: 10.2514/1.A32813

[2] A. Flores-Abad, O. Ma, K. Pham, S. Ulrich, "A review of space robotics technologies for on-orbit servicing", *Progress in Aerospace Sciences*, vol. 68, pp.1-26, 2014, doi: 10.1016/j.paerosci.2014.03.0022.

[3] Y.K. Nakka, W. Hönig, C. Choi, A. Harvard, A. Rahmani and S.-J. Chung, "Information-Based Guidance and Control Architecture for Multi-Spacecraft On-Orbit Inspection", *Journal of Guidance, Control, and Dynamics*, doi:10.2514/1.G006278

[4] B. Bernhard, C. Choi, A. Rahmani, S.J. Chung, F. Hadaegh, "Coordinated Motion Planning for On-Orbit Satellite Inspection using a Swarm of Small-Spacecraft", In *IEEE Aerospace Conference* 2020.

[5] A. Seddaoui, C.Saaj "Combined Nonlinear H-infinity Controller for a Controlled-Floating Space Robot", In emphJournal of Guidance, Control, and Dynamics 2019

[6] J. Zhao,S. Jiang, F. Xie, X. Wang, Z. Li, "Adaptive dynamic sliding mode control for space manipulator with external disturbance.", In emphJournal of Control and Decisions 2018

[7] P. Huang, D. Wang, Z. Meng, F. Zhang,J. Guo, "Adaptive Post-capture Back-stepping Control for Tumbling Tethered Space Robot–Target Combination", *Journal of Guidance, Control, and Dynamics*, vol.39 , pp.150-156, 2016, doi: 10.2514/1.G001309.

[8] W Luo, Y.C. Chu and K-V Ling, "Inverse optimal adaptive control for attitude tracking of spacecraft", *IEEE Transactions on Automatic Control*, vol. 50, pp.1639-1654, 2005.

[9] Jasim Ahmed, Vincent T. Coppola, Dennis S. Bernstein, "Asymptotic Tracking of Spacecraft Attitude Motion with Inertia Matrix Identification", In *Proceedings of the 36th Conference on Decision and Control* 1997

[10] K. Zeyu, Q. Shen, S. Wu, C.J. Damaren, "Saturated Attitude Control of Multi-spacecraft Systems on SO(3) Subject to Mixed Attitude Constraints With Arbitrary Initial Attitude", *IEEE Transactions on Aerospace and Electronic Systems* 2023.

[11] W. Yulin, T. Shengjing, Gu. Jie, W. Xiao, Liu. Chao "Fuzzy-Logic-Based Fixed-Time Geometric Back-stepping Control on SO(3) For Spacecraft Attitude Tracking", *IEEE Transactions on Aerospace and Electronic Systems* 2019.

[12] C.Garanayak, "Robust Adaptive Finite-Time Attitude Tracking with an unknown Inertia Matrix and Disturbance", *2024 IEEE 18th International Conference on Control and Automation (ICCA)* 2024.

[13] A. Nocerino, R. Opromolla, G. Fasano and M. Grassi, "LIDAR-based multi-step approach for relative state and inertia parameters determination of an uncooperative target", *Acta Astronautica*., vol. 181, pp. 662-678, 2021.

[14] M. Mammarella, C. Donati, F. Dabbene, C. Novara and C. Lagoa, "A blended physics-based and black-box identification approach for spacecraft inertia estimation", In *IEEE 63rd CDC* 2024.

[15] M. O'Connor, B. Tweddle, J. Katz, A. Saenz-Otero, D. Miller, K. Makowka, "Visual-Inertial Estimation and Control for Inspection of a Tumbling Spacecraft: Experimental Results from the International Space Station", In *AIAA Guidance, Navigation, and Control Conference*, doi:10.2514/6.2012-4701

[16] M. Lavagna, V. Pesce, and R. Bevilacqua, "Uncooperative objects pose, motion and inertia tensor estimation via stere-ovision", In *ASTRA* 2015.

[17] T. Lee, "Geometric tracking control of the attitude dynamics of a rigid body on SO(3)", In *Proceedings of the 2011 American Control Conference* 2011.

[18] F. Bullo, A.D. Lewis, "Geometric Control of Mechanical Systems-Modeling, Analysis, and Design for Simple Mechanical Control Systems", *Springer New York, NY* 2004.

[19] W.M.Haddad and V.Chellaboina, "Nonlinear Dynamical Systems and Control: A Lyapunov Based Approach", *Princeton, NJ: Princeton University Press* 2008.

[20] H. K. Khalil, "Nonlinear Systems, 3rd ed.", *Upper Saddle River, NJ: Prentice-Hall* 2002.

[21] Ron Larson, Bruce H. Edwards, "Calculus", *Cengage Learning* 2015.

[22] Sanjay P. Bhat a , Dennis S. Bernstein, "A topological obstruction to continuous global stabilization of rotational motion and the unwinding phenomenon" *System and Control Letters* 2000.